Geophysical Journal International Advance Access published August 25, 2016

Magnetic signature of overbank sediment in industry impacted floodplains identified by data mining methods

Monika CHUDANIČOVÁ[a,*], Simon M. HUTCHINSON[b]

[a]Department of Physical Geography and Geoecology, University of Ostrava, Chittussiho 10, 710 00 Ostrava, Czech Republic

m.chudanicova@gmail.com

[b]School of Environment & Life Sciences, University of Salford, Salford, M5 4WT, United Kingdom

s.m.hutchinson@salford.ac.uk

[*]Corresponding author

Monika CHUDANIČOVÁ

Email: m.chudanicova@gmail.com

Telephone: +420777010641

Abbreviated title: Magnetic signature of industry impacted overbank sediments

Summary

Our study attempts to identify a characteristic magnetic signature of overbank sediments exhibiting anthropogenically induced magnetic enhancement and thereby to distinguish them from unenhanced sediments with weak magnetic background values, using a novel approach based on data mining methods, thus providing a mean of rapid pollution determination. Data were obtained from 539 bulk samples from vertical profiles through overbank sediment, collected on seven rivers in the eastern Czech Republic and three rivers in northwest England. K-means clustering and hierarchical clustering methods, paired group (UPGMA) and Ward's method, were used to divide the samples to natural groups according to their attributes. Interparametric ratios: SIRM/χ; SIRM/ARM; and $S_{-0.1T}$ were chosen as attributes for analyses making the resultant model more widely applicable as magnetic concentrations values can differ by two orders. Division into three clusters appeared to be optimal and corresponded to inherent clusters in the data scatter. Clustering managed to separate samples with relatively weak anthropogenically induced enhancement, relatively strong anthropogenically induced enhancement and samples lacking enhancement. To describe the clusters explicitly and thus obtain a discrete magnetic signature, classification rules (JRip method) and decision trees (J4.8 and Simple Cart methods) were used. Samples lacking anthropogenic enhancement typically exhibited an $S_{-0.1T}$ < c. 0.5, SIRM/ARM < c. 150 and SIRM/χ < c. 6000 A . m^{-1}. Samples with magnetic enhancement all exhibited an $S_{-0.1T}$ > 0.5. Samples with relatively stronger anthropogenic enhancement were unequivocally distinguished from the samples with weaker enhancement by an SIRM/ARM > c. 150. Samples with SIRM/ARM in a range c. 126-150 were classified as relatively strongly enhanced when their SIRM/χ > 18,000 A . m^{-1} and relatively less enhanced

when their SIRM/χ < 18,000 A . m^{-1}. An additional rule was arbitrary added to exclude samples with $\chi_{fd\%}$ > 6 % from anthropogenically enhanced clusters as samples with natural magnetic enhancement. The characteristics of the clusters resulted mainly from the relationship between SIRM/ARM and the $S_{-0.1T}$, and SIRM/χ and the $S_{-0.1T}$. Both SIRM/ARM and SIRM/χ increase with increasing $S_{-0.1T}$ values reflecting a greater level of anthropogenic magnetic particles. Overall, data mining methods demonstrated good potential for utilisation in environmental magnetism.

Keywords: Environmental magnetism, Clustering, Statistical methods, Europe

1. Introduction

A range of human activities (e.g. combustion processes, road traffic and industrial effluents) have been identified as sources of ferrimagnetic particles (Petrovský et al. 2000). Of these, the widespread impact of fossil fuel combustion is the most significant (Evans & Heller 2003). Magnetite and magnetite-like minerals originate at high temperatures from pyrite (Flanders 1994) which has an accessorial occurrence in coal (Chaddha & Seehra 1983). Magnetite-rich particles produced by combustion are typically spherical and have been observed by SEM (scanning electron microscopy) in coal-fired power plant fly ash, industrial fly ash and lagooned ash (e.g. Blaha et al. 2008; Jordanova et al. 2006; Magiera et al. 2011). The magnetic enhancement of soils and surfaces due to the presence of magnetic spherules has been reported in the USA and UK (Flanders 1994), Hungary (Zajzon et al. 2013), India (Sharma & Tripathi

2008) in a range of contexts. Magnetic parameters have also been used for the assessment of pollution in fluvial sediments, and soil pollution mapping and assessment in the Czech Republic, Poland, Germany and UK (Crosby et al, 2014; Heller et al. 1998; Kapička et al. 1999; Magiera et al. 2006; Novakova et al. 2012; Petrovský et al. 2000). However, ferrimagnetic material can also be natural in origin. Ferrimagnetic particles can be derived from rocks, originate in pedogenetic processes, be formed by ground fires in clay-rich soils and be produced by bacteria (Thompson & Oldfield 1986). Therefore, it is important, especially for the application of mineral magnetic techniques as chronometers and tracers, to distinguish magnetic enhancement caused by anthropogenic activities from that of natural origins.

Ferrimagnetic particles of anthropogenic origin are typically multidomain (MD) or pseudo-single domain (PSD) in size (Walden et al. 1999) and have a low frequency-dependent susceptibility ($\chi_{fd\%}$), typically below 3 % (Evans & Heller 2003; Hay et al. 1997). Nevertheless, the same characteristics are also valid for some rock derived particles (Walden et al. 1999). The absolute values of magnetic concentration parameters, such as magnetic susceptibility (χ), of samples with anthropogenic magnetic enhancement can vary by an order of two (Evans & Heller 2003). Furthermore, obtaining direct evidence for anthropogenic ferriparticles in large sets of samples using SEM is time consuming and expensive. Thus, a ready means of determining a set of parameters distinguishing anthropogenically enhanced layers of sediment or soil would be highly beneficial. Oldfield (2007) used a combination of different quotients of fundamental magnetic parameters to discriminate between sediment dominated by magnetic minerals formed through pedogenesis and sediment where the dominant content was derived from bacterial magnetite. Oldfield & Crowther (2007)

presented a distinctive magnetic signature for soils with fire induced magnetic enhancement.

The aim of this paper is to determine a distinctive magnetic signature for layers of floodplain sediment with anthropogenically induced magnetic enhancement, using cluster analyses and other data mining methods. Cluster analyses have been used to divide samples into inherent groups in various environmental studies (e.g. Hanesch et al. 2001; Razik et al. 2015; Dekov et al. 1999; Brown & Pasternack 2004).

The magnetic parameters included in this study are a common form of analysis, typically used in many environmental studies. The identification of a distinctive signature differentiating anthropogenic magnetic enhancement would be highly beneficial in both pollution assessment and pollution tracing studies, and research concerned with the investigation of sedimentary records of historical or legacy industrial discharges, especially in the context of on-going and future climate change and the consequences for fluvial systems and floodplain management.

2. Materials and methods

2.1 Study areas and materials

Data for this study was obtained from 539 bulk samples of recent floodplain sediment collected in two European regions. Chudaničová et al. (2016) provide further details of the site characteristics and context. Seven rivers (the Lučina River, Morava River, Odra River, Olše River, Opava River, Petrůvka River and Stonávka River) in the eastern part of the Czech Republic were sampled and 22 profiles were obtained. A subset of 8 profiles (including one profile from each river and two from the Lučina River), where a full set of mineral magnetic parameters were determined,

was used in this study (see Fig. 1). Three rivers (the Ashop River, River Ribble and River Tame) were sampled in northwest England and one profile was obtained from each (see Fig. 2). The catchments of all the Czech rivers sampled comprise predominantly sedimentary rocks, in particular sandstone, mudstone and loess loam. Shale, greywacke and siltstone prevail in the Morava and the Odra Rivers' catchments. Metamorphic rocks including quartzite, amphibolite, schist and gneiss, and to a much lesser extent granite, are present in the headwaters of the Morava and the Opava Rivers (Czech Geological Survey, 2015). The catchments of the northwest England sites comprise predominantly sedimentary rocks; mudstone, siltstone, sandstone and conglomerate prevail (British Geological Survey, 2015).

[Insert Fig. 1]

[Insert Fig. 2]

All the sites are situated in regions influenced by present or former industrial activities. Northwest England was an important centre of the Industrial Revolution in the UK with Manchester being a centre of textile industry and engineering. Sheffield was a centre of steel making industry which therefore lead to a high concentration of coal burning furnaces (Marshall 1974). The eastern part of the Czech Republic lies in the Upper Silesia region, which has high air pollution caused by extensive heavy industry. There are several steelworks which are still active (see Fig. 1). Particularly in the winter period high atmospheric concentrations of fly ash are reported (Czech Statistical Office 2015). Fly ash collected on PM10 filters at a meteorological station in Ostrava (located centrally within the study region), has been found to be highly magnetic. Its magnetic concentration (measured as SIRM; see below) is positively correlated with the content of fly ash/dust collected on the filters (see Fig. 3).

[Insert Fig. 3]

The floodplain samples were collected as contiguous samples at 2.5 cm intervals in vertical profiles in river bank exposures. Bank exposures sit above the present day river bed. Sites were preferentially selected in naturally meandering river sections with minimal local anthropogenic impact. Profiles L5 and OL1 were obtained from re-naturalised sections of rivers which had been straightened in the past. The Czech sites were chosen across the whole region, some in close vicinity to the industrial sources, some on the periphery. All the sampled rivers are aggrading, therefore, their sedimentary record reflects the characteristics of the sediment deposited during recent floods. Sedimentation can also occur through atmospheric in situ deposition, however, this is considered to be of minor influence on the sedimentary record.

In all the sampled profiles, including also those from Chudaničová et al. (2016) which are not presented in this study, magnetic enhancement typically marks out the upper part of the profiles. Fig. 4a shows the depth profiles of χ. Saturation isothermal remanent magnetisation (SIRM) and anhysteretic remanent magnetisation (ARM) are not presented, however, they exhibit the same trend as χ and correlation coefficients between them exceed 0.9 in all cases. The enhancement was identified as anthropogenically induced. The catchments of all the sampled rivers are composed predominantly of sedimentary strata, with limited exposures of metamorphic rocks. Both are magnetically weak and published values for these rocks (Dearing 1999) correspond to the background values at depth in the profiles where the sedimentary record extends beyond the zone of enhancement (L2, OD1, OP2, P1). Magnetic enhancement originating through pedogenesis or fire can be excluded, because enhancement of this origin produces superparamagnetic (SP) grains which are distinguishable by

high $\chi_{fd\%}$ values (> 6 %) (Dearing et al. 1996); the magnetically enhanced layers of the profiles used in this study have a low $\chi_{fd\%}$ (see Fig. 4b). Bacterial activity can also be excluded as a source of magnetic enhancement as significant ARM values, typical for bacterial magnetite (Maher 1988), were absent. Furthermore, the magnetic enhancement observed in the profiles shows increased $S_{-0.1T}$values indicating an increase in magnetically soft minerals, such as magnetite (Walden et al. 1999) (see Fig. 4e). Finally, spherules, typical of particles derived by combustion were observed in the samples using SEM. Concentrations of Pb and Zn follow similar trends as χ (see Fig. 4c-d) which also supports an anthropogenic origin of the magnetic enhancement.

[Insert Fig. 4]

Some of the profiles are magnetically enhanced throughout the profile (see Fig. 4a) reflecting higher sedimentation rates (e.g. profile M3) or a longer pollution history (UK profiles - RR, RT). Profiles L5 and OL1 may have been directly influenced by steelworks effluents because they are located downstream from ArcelorMittal Ostrava and Třinecké železárny steelworks. Small rusty iron fragments were found in profile S1. Extreme values of Pb and Zn concentration at depth in profile L5 are caused by leaching from a degrading plastic wrapper found there. For further information about the data see Table 1 and Chudaničová et al. (2016).

In the following text, samples or layers are described as follows - e.g. S1 50, where S1 is label of a profile and S is derived from a river's name (e.g. the Stonávka River, see Table 1) and 50 is the depth of the sample within the profile (cm). Two numbers connected with hyphen, e.g. 2.5-40, refer to a layer between these depths.

[Insert Table 1]

2.2 Rock magnetic methods

All samples were oven dried at 40 °C and gently crushed prior to analyses. Dried and powdered samples were then packed into 10 cm^3 plastic pots and immobilised. χ, ARM and IRM measurements (in this order) were performed. χ and $\chi_{fd\%}$ were measured in a Bartington Instruments Ltd MS2B sensor. χ is a low field magnetic susceptibility. ARM was imparted in a Molspin AF demagnetizer with a maximum field of 100 mT and a steady bias field of 0.04 mT. IRM was imparted by a Molspin pulse magnetiser in fields of 1 T, -20 mT, -40 mT, -100 mT and -300 mT. After magnetisation, magnetic remanences were measured in a Minispin fluxgate magnetometer.

SIRM is defined as IRM measured in 1 T field. S-ratio was calculated as -IRM_{-100mT}/SIRM and therefore is labelled as $S_{-0.1T}$. This is a standard formula for S-ratio, proposed by Thompson & Oldfield (1986) and Walden et al. (1999) although other formulae may be used to calculate S-ratio, e.g. -IRM_{-300mT}/SIRM. However, both reflect the proportion of magnetite to haematite in a mixture as shown in an experiment by Frank & Nowaczyk (2008).

2.3 Data mining methods

As an analysis input, relative parameter ratios were preferred to the absolute values of χ_{lf}, SIRM and ARM. Absolute values themselves may not be a good indicator of magnetic enhancement as they are influenced by a sample's source geology. The magnetic background values of the sites also differ reflecting differences in local geology. The advantage of employing relative parameter ratios is also in the wider applicability of the resultant model. The quotients chosen as attributes were SIRM/χ, SIRM/ARM, $S_{-0.1T}$ and $\chi_{fd\%}$; $\chi_{fd\%}$ is defined by Dearing (1999) as $(\chi_{lf} - \chi_{hf})/\chi_{lf}$ where χ_{lf} is low

frequency susceptibility and χ_{hf} is high frequency susceptibility. Depth profiles of SIRM/χ, SIRM/ARM, $S_{-0.1T}$ and $\chi_{fd\%}$ of all the samples sites are presented in Fig. 4.

K-means clustering and hierarchical clustering methods, paired group (UPGMA) and Ward's method, were performed using PAST software (Hammer et al. 2001). Clustering techniques divide instances into natural groups based on the instances' attributes. For k-means clustering, the number of clusters (k) is selected prior to analysis. K points are randomly selected in an instance space to be cluster centres. Instances are then iteratively joined to their closest cluster centre and form clusters. Every time an instance is joined to a cluster centre, a new cluster centre is calculated in order to minimise the total squared distance from each of the cluster's points to its centre. The clustering process is complete when the cluster centres have stabilised. Hierarchical clustering creates dendrograms (tree diagrams). Similar instances are joined together to form small clusters which are then gradually joined into larger ones and thus a hierarchical, tree structure, is created (Witten & Frank 2005).

For clustering algorithms, the Euclidean distance was used in formulas. However, the Euclidean distance is not suitable where the attributes have different scales because those with larger scales dominate in clustering, whereas attributes with smaller scales become insignificant (Witten & Frank 2005). For this reason, all attributes were normalised in WEKA (Hall et al. 2009) to lie within the interval [0, 1], prior to analyses. Formula for normalisation is as follows: $a_i = (v_i - \min v_i)/(\max v_i - \min v_i)$, where v_i is the actual value of attribute i, and the maximum and minimum are taken over all instances in the data set (Witten & Frank 2005).

Outliers in data may influence results of cluster analyses, therefore, it is important to discard them (Witten & Frank 2005). Only sample S1 50, with

very high value of SIRM/χ, compared to other samples, and sample P1 125 with extremely high, possibly erroneous value of $\chi_{fd\%}$ were removed from our dataset prior to analyses. Negative, and thus erroneous, values of $\chi_{fd\%}$ were replaced by 0.

Clustering was followed by the building of a classification model to obtain an explicit description of clusters. Classification rules were generated using the JRip method and decision trees were built by J4.8 and Simple Cart methods. All classifications were carried out in WEKA.

3. Results

After multiple runs of k-means cluster analysis with various k values, it was found that $\chi_{fd\%}$ does not significantly influence final clusters and causes higher errors in the classification models when included. Clustering was also unable to distinguish the only layer within the samples thought to exhibit natural magnetic enhancement (AR 55-92.2) and with a high $\chi_{fd\%}$. Only UPGMA algorithm was able to distinguish layer AR 65-92.5 along with samples L 80 and L 90 as a separate branch in its dendrogram. This generally poor performance is probably a result of the influence of magnetically weak samples in profile L2 and OP2 which fluctuate highly in $\chi_{fd\%}$, from negative values up to 8 % (see Fig. 4b). Measurements of the χ of magnetically weak samples are prone to significant influences caused by environmental influences on the measurements and thus calculated $\chi_{fd\%}$ values can be unreliable (Dearing 1999). Therefore, it was decided to exclude $\chi_{fd\%}$ from analyses and arbitrarily add an additional rule based on our reservations about the reliability of this parameter as a discriminator. This rule excludes samples with $\chi_{fd\%}$ higher than 6 % (Dearing & Bird 1997) from the categories identified as displaying anthropogenically induced

magnetic enhancement. Thus all the models presented do not include the attribute $\chi_{fd\%}$.

K-means clustering where k=2 divides the samples into two clusters (see Fig.5). Cluster 2 contains the whole of profiles L5, OL1, RT and S1. They all exhibit strong magnetic enhancement and high values of both χ and SIRM. As mentioned earlier, sediments in profiles L5 and OL1 may have been influenced by steelworks effluents, small fragments of rusty iron were found in S1 and RT comes from a river within the urban area of Greater Manchester. Also included are most of the magnetically enhanced layer in profile L2 (2.5-30), the upper 87.5 cm of RR and several samples from P1 - the samples with the highest SIRM values and a relatively high χ. Cluster 1 includes the whole of profiles AR, M3, OD1, OP2 and the remaining samples from profiles L2, P1 and RR. Therefore, cluster 1 consists of samples which lack any marked magnetic enhancement and the magnetically enhanced layers of sites more remote from pollution sources (see Fig. 5).

[Insert Fig. 5]

When k is increased to 3, profiles L5, OL1, RT and S1 remain in cluster 2. Samples from L2 and one sample of RR are moved to the cluster 1. Cluster 1 contains magnetically enhanced samples where the enhancement is relatively low compared to that of the samples in the cluster 2. Cluster 3 comprises layers of L2, OP2, OD1 and P1 where there is no magnetic enhancement, and the bottom layer of profile AR (see Fig. 5).

Further increases in k cause the subdivision of former clusters into subclusters and other minor changes within clusters and does not assist in any meaningful sample discrimination.

Using only three parameters for the clustering enables to visualise the data scatter in a pseudo 3D plot. Fig. 6 shows that data points are grouped into approx. three natural clusters. The Elbow method was also applied to find an optimal number of k for k-means clustering. This method is based on plotting average within cluster squared distance W_k against number of k used. W_k decreases monotonically with increasing k but from a point called as 'elbow' the decrease flattens markedly. This 'elbow' is considered to be the optimal number of clusters (e.g. Tibshirani et al. 2001). Fig. 7 confirms that three is an optimal number of clusters and gives a right balance between describing the most of variability within data and number of clusters.

[Insert Fig. 6]

[Insert Fig. 7]

The results of hierarchical clustering UPGMA are shown in Fig. 8. Only the main branches at the first few upper levels of the dendrogram are presented. The full dendrogram is provided in the supplementary materials. The UPGMA method differentiates three main branches at the first level of dendrogram. The first branch of the dendrogram includes the whole of profile OL1, RT, L5 (except sample 95) and S1, and most of profile RR (2.5-87.5). Similarly, as in cluster 2 this branch contains samples exhibiting strong magnetic enhancement. The next branch of the dendrogram contains samples L2 45-160, OD1 70-115, OP2 27.5-150, P1 117.5-132.5 and AR 85, 95, 100-110. These samples can be described as samples with natural or background mineral magnetic characteristics. The last branch includes the rest of the samples: the whole of profileM3, plus P1 2.5-115, RR 90-95, AR 2.5-82.5, 87.5-92.5, 97.5, OD1 2.5-67.5, OP2 2.5-25, L2 2.5-42.5, L5 95. These samples can be described as samples with a relatively lower level of enhancement than that of the samples in the first

branch. The three main branches of the dendrogram were treated as three clusters (see Fig. 8) and the numbering 1-3 corresponds to that of the k-means clustering; cluster 1 represents samples with relatively weak magnetic enhancement; cluster 2 represent samples with relatively strong magnetic enhancement and cluster 3 contain samples lacking enhancement.

Ward's method also produces three main branches which contain almost the same set of samples as the three branches of UPGMA and three clusters of k-means, therefore its results are not presented here (only in Figure 10). The full dendrogram can be found in the supplementary materials.

[Insert Fig. 8]

The resultant clusters produced by k-means and UPGMA are presented graphically in Fig. 9 and 10. Figure 10 also includes the Ward's method. Both figures show that all three clustering methods produced very similar results.

[Insert Fig. 9]

[Insert Fig. 10]

In order to obtain an explicit description of the clusters, classification models were created using classification rules (JRip method) and decision trees (J4.8 and Simple Cart). Classification creates a set of rules which classify samples/instances into appropriate clusters, respectively predict an appropriate cluster for each combination of attributes. For each of the three sets of clusters created by the clustering methods a single classification model was created using the JRip method and two classification models were created using decision trees (J4.8 and Simple Cart). Therefore, in total nine models were obtained. Figure 11 shows

Simple Cart models for k-means and UPGMA clusters. Classification rules and J4.8 trees can be found in the supplementary materials. All nine models exhibit low errors, i.e. below 3 %, and thus can be considered as a good description of clusters.

[Insert Fig. 11]

All the models describe the clusters in a similar way. Cluster 3 is unequivocally distinguished by $S_{-0.1T} < \sim 0.5$. Typically SIRM/ARM is $< \sim 150$ and SIRM/$\chi < \sim 6000$ A . m^{-1}. Few samples belonging to cluster 3 have SIRM/ARM > 150, those have S-ratio < 0.6. Virtually all samples with $S_{-0.1T} > \sim 0.5$ belong to clusters 1 and 2. Cluster 1 is described as having SIRM/ARM $< \sim 126$ or having SIRM/ARM $< \sim 150$ and SIRM/$\chi < \sim 18{,}000$ A . m^{-1} (this value for SIRM/χ ranges from 11,000 to about 20,000 A . m^{-1} across the classification models). Samples in cluster 2 then have SIRM/ARM $> \sim 150$. Some have a little lower SIRM/ARM , approx. 126-150, in this case SIRM/$\chi > \sim 18{,}000$ A . m^{-1}. These rules fail to classify correctly 10 samples on average.

4. Discussion

All the cluster analyses were able to separate samples with natural or background mineral magnetic characteristics from those displaying anthropogenic magnetic enhancement. The anthropogenically influenced samples were divided into two clusters; one containing samples with strong enhancement, potentially influenced by steelworks effluents or iron fragments; the other including samples with weaker enhancement. All the clustering methods produced comparable results and created clusters/branches corresponding to natural clusters in the dataset (see Fig. 9).

Because magnetic parameter quotients were preferred to absolute values, clustering performs well, although samples from a range of sites were included. This is corroborated by the correct assignment of the upper layer of profile AR as anthropogenically influenced, although its χ values are in the range of the background characteristics of the other sites. In the case of AR, χ has probably been lowered by the high organic matter content of the samples demonstrated by the LOI (loss-on-ignition, Dean 1974) values (see Table 1) as significant peat erosion has been reported on the moorlands of AR's catchment (Tallis 1985; Hutchinson 1995; Holden 2007).

The only layer within the samples displaying natural magnetic enhancement and elevated $\chi_{fd\%}$, AR 55-92.5, was not clearly identified, although $\chi_{fd\%}$ was included in first runs of the analyses. The inability to identify this layer was probably caused by magnetically weak samples from profiles L2 and OP2 with unreliable values of $\chi_{fd\%}$ (Dearing 1999).

[Insert Fig. 12]

[Insert Fig. 13]

The mineral magnetic signature described by particular clusters is based predominantly on the relationships in Figs 12 and 12. The $S_{-0,1T}$ of samples showing magnetic background characteristics ranges from 0.1 to 0.5 which, according to Frank & Nowaczyk (2008), indicates that the remanence carrying fraction contains over 90 % haematite or other imperfect antiferromagnetic minerals. Nevertheless, most of the remanence is still carried by ferrimagnetic minerals. SIRM/χ is approximately constant and low. In samples with a high content of imperfect antiferromagnetic minerals it should be relatively increased (Oldfield 1991). However, when mixed with a significant amount of paramagnetic material, which is the case here, values of SIRM/χ are lowered because, in absence of strong

ferrimagnetic minerals, paramagnetic material significantly increases χ but has no influence on SIRM (Walden et al. 1999). The constancy of SIRM/χ also indicates that there is no magnetic grain size influence and a MD grain size dominates (Thompson & Oldfield 1986). The SIRM/ARM ratio is different and varies significantly in the samples with low $S_{-0.1T}$. These samples can be seen to be scattered in the plot in Fig. 13. Frank & Nowaczyk (2008) mention the data scatter of ARM-based parameters and explain it by the incomplete saturation of haematite in ARM acquisition fields.

In the anthropogenically enhanced samples, when the $S_{-0.1T}$ is greater than 0.5, the SIRM/χ and the SIRM/ARM ratios increase with increasing $S_{-0.1T}$ reflecting the increasing content of anthropogenic ferrimagnetic particles. However, according to the literature, samples where ferrimagnetic material/magnetite are dominant should have a low SIRM/χ (Oldfield 1991; Walden et al. 1999). This was also experimentally proven by Frank & Nowaczyk (2008) on mixtures of crushed magnetite and haematite. They found that with an increasing content of magnetite (and S-ratio), SIRM/χ decreases. The SIRM/ARM ratio is presented in literature as a grain size indicator (Thompson & Oldfield 1986) or in susceptibility form (χ_{ARM}) as a fine-grained magnetite indicator (Maher 1988). Nevertheless, combustion derived spherules are not a stoichiometric magnetite and may contain Al substitutions (Jordanova et al. 2004). Due to rapid cooling as they are formed, high stresses occur inside the grains which make them magnetically harder than crushed or grown magnetite (Flanders 1999; Jordanova et al. 2006). The internal structure of magnetic spherules is also very complex and might influence magnetic parameters (Jordanova et al. 2004). Blaha et al. (2008) describe spherules analysed by SEM/EDX analysis as consisting of large magnetite crystals in a glassy matrix or more uniform,

fine magnetite crystals within a glassy matrix. The glassy matrix has a low iron content, but higher levels of Si, Al and Ca. Al, Si or other elements concentrated within the spherules' structures or stuck on their surface were reported also by e.g. Magiera et al. (2011) and Jordanova et al. (2006).

An alternative explanation for the high SIRM/χ and SIRM/ARM, and their relationship with $S_{-0.1T}$ may be grain interaction effects. Lees (1997) considered grain interactions as a possible source of linear non-additivity in mixtures of environmental materials. In particular mixtures with highly ferrimagnetic materials such as chimney slag exhibited the highest non-additivity phenomena. These phenomena were regarded as especially significant in remanence measurements. Whereas the χ of a mixture was the same as expected according to the χ of the mixture's sources, the SIRM of the mixtures was higher than expected.

Some interactions were observed while obtaining a magnetic extract from our samples for SEM observations and later on in the SEM images. In addition to magnetic spherules, angular particles of similar sizes were extracted by hand magnet in an isopropyl alcohol suspension. These are probably particles of floodplain sediment, containing high amounts of Al, Si, C and also Fe and O (see Fig. 14). In the SEM observations they were mostly clustered with the spherules (see Fig. 15). In the absence of magnetic spherules, only negligible quantities of these particles were extracted by this method.

[Insert Fig. 14]

[Insert Fig. 15]

Similarly high values of SIRM/χ and SIRM/ARM ratios were also reported by Hay et al. (1997) in anthropogenically polluted UK topsoils, high values of

SIRM/χ were reported for fly ash samples from coal burning power plants by Magiera et al. (2011), and high values of SIRM/ARM were reported by Hutchinson (1993) in saltmarsh sediments influenced by steel works.

Samples in the upper left corner of the plot in Figs 12 and 13 do not fit the general trend. They are the samples of naturally enhanced layer in profile AR with a high $\chi_{fd\%}$. SIRM/χ is low reflecting the SP size of the magnetic grains. SP grains increase χ whereas SIRM is not affected (Oldfield 1991; Thompson & Oldfield 1986). Further insight into the relationships in the plots (Figs 12 and 13) is not possible without further analyses, e.g. IRM acquisition curves, coercivity-related parameters or temperature dependent susceptibility.

5. Conclusions

All the cluster analyses employed were successful in distinguishing anthropogenic magnetically enhanced samples from those lacking enhancement implying that both categories have their own distinctive magnetic signature. Classification methods explicitly described the clusters in an efficient way, with errors lower than 3 %, providing a set of rules to identify samples with anthropogenic magnetic enhancement. These rules were predominantly based on relationships between SIRM/χ, SIRM/ARM and $S_{-0.1T}$. Both SIRM/χ and SIRM/ARM increase with increasing $S_{-0.1T}$, i.e. with the increasing content of anthropogenically derived ferrimagnetic spherules. This is contrary to some experimental studies, however may be explained by impurities in the spherules or grain interaction effects. The inclusion of $\chi_{fd\%}$ in analyses was problematic. Thus an arbitrary rule was added which excluded all samples with $\chi_{fd\%} > 6$ % from categories of anthropogenic magnetic enhancement. The approach presented provides a

simple and effective way to identify anthropogenically influenced sediments.

It cannot be stated that rules of classification models are generally applicable for all samples from various geological conditions. The samples used for this study are floodplain sediment samples coming from catchments comprising more or less magnetically weak sedimentary rocks.

6. Acknowledgement

The authors are grateful to Renata Vojkovská (University of Ostrava) who supervised the SEM analysis. We would like to thank the reviewers of our manuscript for their careful and thoughtful insights which have enhanced this submission. This study was supported by University of Ostrava [grant number SGS18/PřF/2015-2016].

References

Blaha, U., Sapkota, B., Appel, E., Stanjek, H. & Rosler, W., 2008. Micro-scale grain-size analysis and magnetic properties of coal-fired power plant fly ash and its relevance for environmental magnetic pollution studies, *Atmos. Environ.*, 42, 8359–8370. doi:10.1016/j.atmosenv.2008.07.051

British Geological Survey, 2015. Online map applications. Available at: www.bgs.ac.uk (accessed January 2014).

Brown, K. J. & Pasternack, G. B., 2004. The geomorphic dynamics and environmental history of an upper deltaic floodplain tract in the

Sacramento-San Joaquin Delta, California, USA, *Earth Surf. Process. Landforms*, 29, 1235-1258. doi: 10.1002/esp.1088

Chaddha, G. & Seehra, M., 1983. Magnetic components and particle size distribution of coal flyash, *J. Phys. D. Appl. Phys.*, 1767.

Chudaničová, M., Hutchinson, S.M., Hradecký, J. & Sedláček, J., 2016. Environmental magnetism as a dating proxy for recent overbank sediments of (peri-)industrial regions in the Czech Republic and UK, *Catena*, 142, 21-35. doi: 10.1016/j.catena.2016.02.008

Crosby, C.J., Fullen, M.A. & Booth, C.A., 2014. Potential linkages between mineral magnetic measurements and urban roadside soil pollution (part 2), *Environ. Sci. Process. Impacts*, 16, 548–557. doi:10.1039/c3em00345k

Czech Geological Survey, 2015. Online map applications. Available at: www.geology.cz/extranet/mapy/mapy-online/mapove-aplikace (accessed November 2013).

Czech Statistical Office, 2015. Online data. Available at: www.czso.cz (accessed January 2014).

Dean, W. E., 1974. Determination of carbonate and organic matter in calcareous sediments and sedimentary rocks by loss on ignition: comparison with other methods, *J. Sediment. Petrol.*, 44, 242-248.

Dearing, J., 1999. *Environmental Magnetic Susceptibility: Using the Bartington MS2 System*, Bartington Instruments, Oxford.

Dearing, J. & Bird, P., 1997. Secondary ferrimagnetic minerals in Welsh soils: a comparison of mineral magnetic detection methods and implications for mineral formation, *Geophys. J. Int.*, 130, 727–736.

Dearing, J., Hay, K., Baban, S., Huddleston, A., Wellington, E. & Loveland, P., 1996. Magnetic susceptibility of soil: an evaluation of conflicting theories using a national data set, *Geophys. J. Int.*, 127, 728–734.

Dekov, V. M., Van Put, A., Eisma, D. & Van Grieken, R., 1995. Single particle analysis of suspended matter in the Makasar Strait and Flores Sea with particular reference to tin-bearing particles, *J. Sea Res.*, 41, 35-53. doi: 10.1016/S1385-1101(98)00035-5

Evans, M.E. & Heller, F., 2003. *Environmental Magnetism: Principles and Applications of Enviromagnetics*, Academic Press, San Diego-London-Burlington.

Flanders, P., 1999. Identifying fly ash at a distance from fossil fuel power stations, *Environ. Sci. Technol.*, 33, 528–532.

Flanders, P.J., 1994. Collection, measurement, and analysis of airborne magnetic particulates from pollution in the environment (invited), *J. Appl. Phys.*, 75, 5931–5936. doi:10.1063/1.355518

Frank, U. & Nowaczyk, N.R., 2008. Mineral magnetic properties of artificial samples systematically mixed from haematite and magnetite, *Geophys. J. Int.*, 175, 449–461. doi:10.1111/j.1365-246X.2008.03821.x

Hall, M., Frank, E., Holmes, G., Pfahringer, B., Reutemann, P. & Witten, I. H., 2009. The WEKA Data Mining Software: An Update, *SIGKDD Explorations*, 11, Issue 1.

Hanesch, M., Scholger, R. & Dekkers, M. J., 2001. The application of fuzzy c-means cluster analysis and non-linear mapping to a soil data set for the detection of polluted sites, *Phys. Chem. Earth*, 26, 11-12.

Hammer, Ø., Harper, D. A. T. & Ryan, P.D., 2001. Paleontological statistics software package for education and data analysis, *Palaeontol. Electron.*, 4, 9–18. doi:10.1016/j.bcp.2008.05.025

Hay, K., Dearing, J., Baban, S. & Loveland, P., 1997. A preliminary attempt to identify atmospherically-derived pollution particles in English topsoils from magnetic susceptibility measurements, *Phys. Chem. Earth*, 22, 207-210. doi:10.1016/S0079-1946(97)00104-3

Heller, F., Strzyszcz, Z. & Magiera, T., 1998. Magnetic record of industrial pollution in forest soils of Upper Silesia, Poland, *J. Geophys. Res.*, 103, 17767-17774. doi:10.1029/98JB01667

Holden, J., Shotbolt, L., Bonn, A., Burt, T.P., Chapman, P.J., Dougill, A.J., Fraser, E.D.G., Hubacek, K., Irvine, B., Kirkby, M.J., Reed, M.S., Prell, C., Stagl, S., Stringer, L.C., Turner, A. & Worrall, F., 2007. Environmental change in moorland landscapes, *Earth-Science Rev.*, 82, 75–100. doi:10.1016/j.earscirev.2007.01.003

Hutchinson, S.M., 1993. The magnetic record of particulate pollution in a saltmarsh, Dee Estuary, UK, *The Holocene*, 3, 342–350. doi:10.1177/095968369300300406

Hutchinson, S. M., 1995. Use of magnetic and radiometric measurements to investigate erosion and sedimentation in a British upland catchment, *Earth Surf. Process. Landforms*, 20, 293 - 314.

Jordanova, D., Hoffmann, V. & Fehr, K.T., 2004. Mineral magnetic characterization of anthropogenic magnetic phases in the Danube river sediments (Bulgarian part), *Earth Planet. Sci. Lett.*, 221, 71–89. doi:10.1016/S0012-821X(04)00074-3

Jordanova, D., Jordanova, N. & Hoffmann, V., 2006. Magnetic mineralogy and grain-size dependence of hysteresis parameters of single spherules from industrial waste products, *Phys. Earth Planet. Inter.*, 154, 255–265. doi:10.1016/j.pepi.2005.06.015

Kapička, A., Petrovský, E., Ustjak, S. & Macháčková, K., 1999. Proxy mapping of fly-ash pollution of soils around a coal-burning power plant: A case study in the Czech Republic, *J. Geochemical Explor.*, 66, 291–297. doi:10.1016/S0375-6742(99)00008-4

Lees, J. A., 1997. Mineral magnetic properties of mixtures of environmental and synthetic materials: linear additivity and interaction effects, *Geophys. J. Int.*, 131, 335–346. doi:10.1111/j.1365-246X.1997.tb01226.x

Magiera, T., Jabłońska, M., Strzyszcz, Z. & Rachwal, M., 2011. Morphological and mineralogical forms of technogenic magnetic particles in industrial dusts, *Atmos. Environ.*, 45, 4281–4290. doi:10.1016/j.atmosenv.2011.04.076

Magiera, T., Strzyszcz, Z., Kapicka, A. & Petrovsky, E., 2006. Discrimination of lithogenic and anthropogenic influences on topsoil magnetic susceptibility in Central Europe, *Geoderma*, 130, 299–311. doi:10.1016/j.geoderma.2005.02.002

Maher, B. A., 1988. Magnetic properties of some synthetic sub-micron magnetites, *Geophys. J.*, 94, 83–96. doi:10.1111/j.1365-246X.1988.tb03429.x

Marshall, J.D., 1974. *Lancashire*, David & Charles, Newton Abbot.

Novakova, T., Grygar, T.M., Babek, O., Famera, M., Mihaljevic, M. & Strnad, L., 2012. Distinguishing regional and local sources of pollution by trace metals and magnetic particles in fluvial sediments of the Morava River,

Czech Republic, *J. Soils Sediments*, 13, 460–473. doi:10.1007/s11368-012-0632-8

Oldfield, F., 2007. Sources of fine-grained magnetic minerals in sediments: a problem revisited, *The Holocene*, 17, 1265–1271.

Oldfield, F., 1991. Environmental magnetism-a personal perspective, *Quat. Sci. Rev.*, 10, 73–85.

Oldfield, F. & Crowther, J., 2007. Establishing fire incidence in temperate soils using magnetic measurements, *Palaeogeogr. Palaeoclimatol. Palaeoecol.*, 249, 362–369. doi:10.1016/j.palaeo.2007.02.007

Petrovský, E., Kapička, A. & Jordanova, N., 2000. Low-field magnetic susceptibility: a proxy method of estimating increased pollution of different environmental systems, *Environ. Geol.*, 39, 1–7.

Razik, S., Govin, A., Chiessi, C. M. & von Dobeneck, T., 2015. Depositional provinces, dispersal, and origin of terrigenous sediments along the SE South American continental margin, *Mar. Geol.*, 363, 261-272. doi:10.1016/j.margeo.2015.03.001

Sharma, A. & Tripathi, B., 2008. Magnetic mapping of fly-ash pollution and heavy metals from soil samples around a point source in a dry tropical environment, *Environ. Monit. Assess.*, 138, 31–39.

Tallis, J.H., 1985. Erosion of blanket peat in the southern Pennines: new light on an old problem, in: Johnson, R.H. (Ed.), *The Geomorphology of North-West England*, Manchester University Press, Manchester, p. 421.

Tibshirani, R., Walther, G. & Hastie, T., 2001. Estimating the number of clusters in a data set via the gap statistic, *J. R. Statist. Soc. B*, 63, 411-423.

Thompson, R. & Oldfield, F., 1986. *Environmental magnetism*, Allen & Unwin, London.

Walden, J., Oldfield, F. & Smith, J., 1999. *Environmental magnetism: a practical guide*, Quaternary Research Association, London.

Witten, I.H. & Frank, E., 2005. *Data Mining: Practical Machine Learning Tools and Techniques*, 2nd ed. Elsevier Inc.

Zajzon, N., Marton, E., Sipos, P., Pethe, M., Nemeth, T., Kovacs-Kis, V. & Uram, J., 2013. Tracking magnetic pollutants by integrated mineralogical and magnetic analyses of airborne particles in urban environment, *Carpathian J. Earth Environ. Sci.*, 8, 221–229.

Figure captions

Fig. 1. Study areas in the Czech Republic depicting sampled sites and their proximity to industrial sources. *Reprinted from Catena, 142, Chudaničová, M., Hutchinson, S.M., Hradecký, J., Sedláček, J., Environmental magnetism as a dating proxy for recent overbank sediments of (peri-)industrial regions in the Czech Republic and UK, 21-35, 2016, with permission from Elsevier.*

Fig. 2. Study areas in the United Kingdom depicting sampled sites. *Reprinted from Catena, 142, Chudaničová, M., Hutchinson, S.M., Hradecký, J., Sedláček, J., Environmental magnetism as a dating proxy for recent overbank sediments of (peri-)industrial regions in the Czech Republic and UK, 21-35, 2016, with permission from Elsevier.*

Fig. 3. Relationship between SIRM (A/m) and mass (μg) of dust collected on PM10 filters in the Ostrava-Poruba meteorological station (eastern Czech Republic). The samples are from the period 1 January - 26 February 2010.

Fig. 4. Depth profiles of the measured parameters: a) magnetic susceptibility (χ), b) frequency-dependent magnetic susceptibility ($\chi_{fd\%}$) (Note: Sample P1 125 with extreme value 20.6 % was discarded from the plot to avoid superimposition of the other values), c) concentration of Pb, d) concentration of Zn, e) $S_{-0.1T}$, f) SIRM/ARM ratio and g) SIRM/χ ratio. *Note: Colour-shaded background indicates samples' affiliation to the resultant three clusters of k-means clustering: Red crosses = cluster 1, blue dots = cluster 2, and green lines and dots = cluster 3.*

Fig. 5. Resultant separation of samples into clusters by the k-means clustering method with k=2 and k=3.

Fig. 6. Pseudo 3D plot visualising the data points' scatter in the clustering space.

Fig. 7. The so-called Elbow method. Average within cluster squared distance decreases with increasing number of clusters (k). The 'elbow' of the curve, in this case number 3, is the optimal number of clusters.

Fig. 8. Simplified dendrograms created by hierarchical clustering method UPGMA. The main branches of the dendrogram are labelled in the same way as the k-means clusters.

Fig. 9. Pseudo 3D plots depicting clusters distinguished by a) k-means clustering and b) UPGMA method.

Fig. 10. Graphical expression of the clusters resulting from all three clustering methods using magnetic quotients.

Fig. 11. Decision trees created by Simple Cart method for a) k-means clusters and b) UPGMA clusters. Note: MAE is the mean absolute error and RMSE is the root-mean-square error. The numbers in brackets indicates the number of samples classified by each tree branch.

Fig. 12. Relationship between SIRM/χ and $S_{-0.1T}$. All samples analysed are included. The key differentiates samples from each profile.

Fig. 13. Relationship between SIRM/ARM and $S_{-0.1T}$. All sampled analysed are included. The key differentiates samples from each profile.

Fig. 14. Energy-dispersive X-ray spectrum of the angular particles in the magnetic extract (visible in Figure 15) obtained using a hand magnet and isopropyl alcohol. Note: Au, Pt and Pd were used for sample coating prior to analysis.

Fig. 15. SEM images showing clusters of spherules originated in combustion processes and angular particles (probably rock fragments) in floodplain sediment. (Magnetic extract for this image was obtained from sample L5 22.5).

Table caption

Table 1. Maximal and minimal values of magnetic parameters and other characteristics of the study profiles.

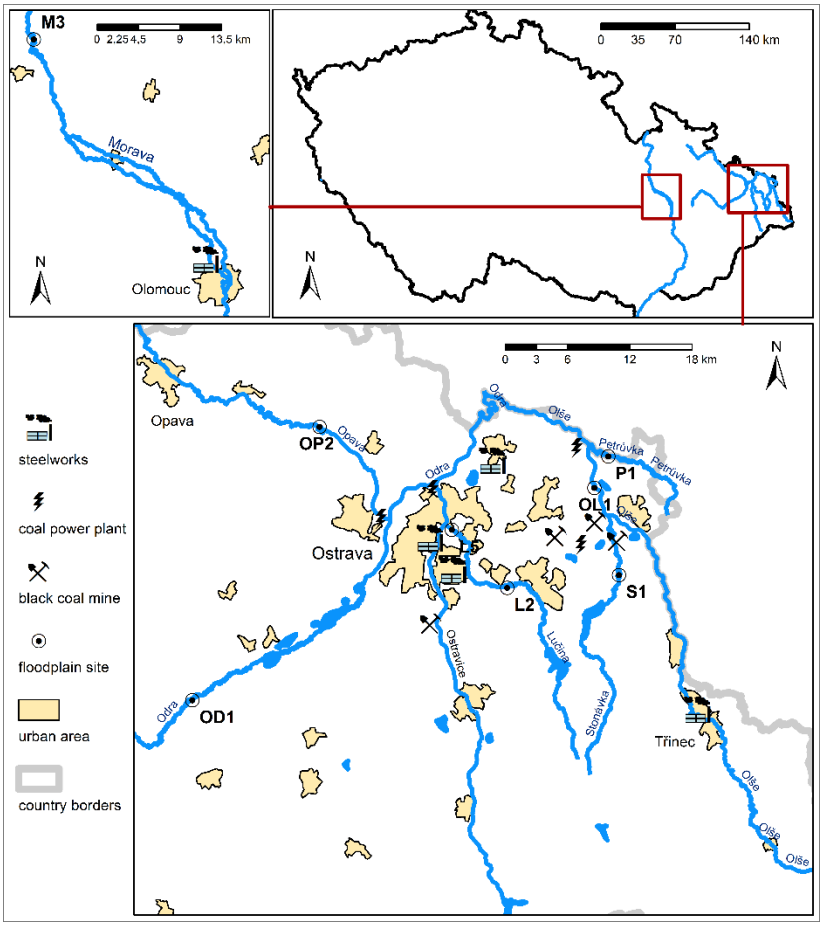

Fig. 1. Study areas in the Czech Republic depicting sampled sites and their proximity to industrial sources. (Reprinted from Catena, 142, Chudaničová, M., Hutchinson, S.M., Hradecký, J., Sedláček, J., Environmental magnetism as a dating proxy for recent overbank sediments of (peri-)industrial regions in the Czech Republic and UK, 21-35, 2016, with permission from Elsevier.)

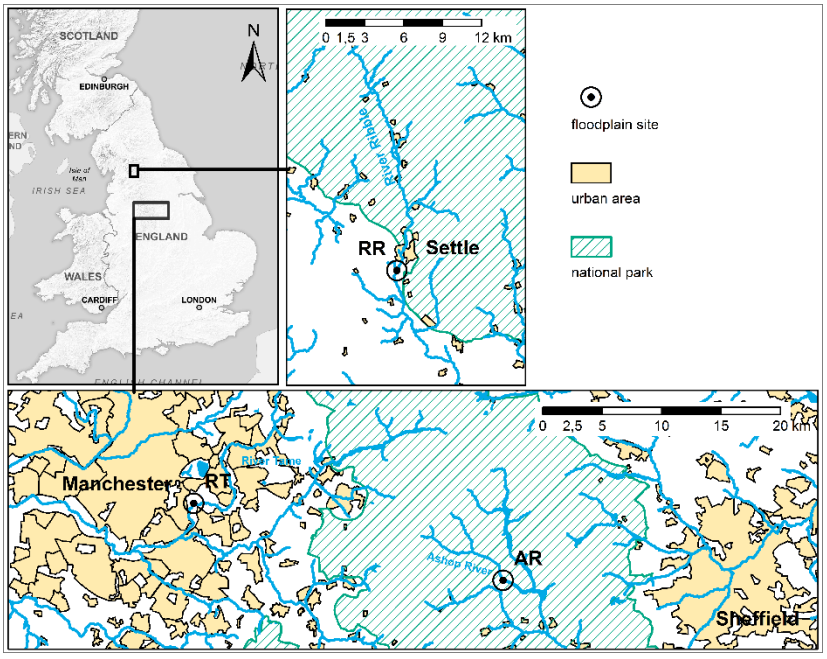

Fig. 2. Study areas in the United Kingdom depicting sampled sites. (Reprinted from Catena, 142, Chudaničová, M., Hutchinson, S.M., Hradecký, J., Sedláček, J.,

Environmental magnetism as a dating proxy for recent overbank sediments of (peri-)industrial regions in the Czech Republic and UK, 21-35, 2016, with permission from Elsevier.)

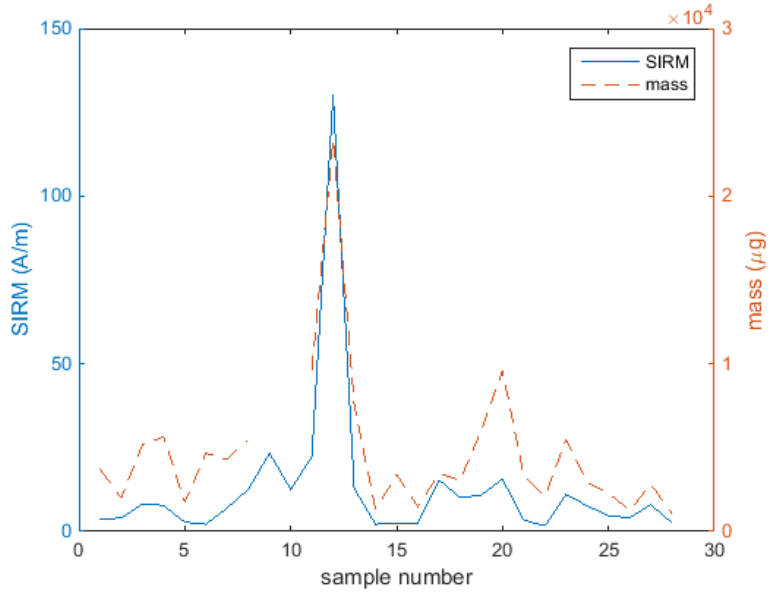

Fig. 3. Relationship between SIRM (A/m) and mass (μg) of dust collected on PM10 filters in the Ostrava-Poruba meteorological station (eastern Czech Republic). The samples are from the period 1 January - 26 February 2010.

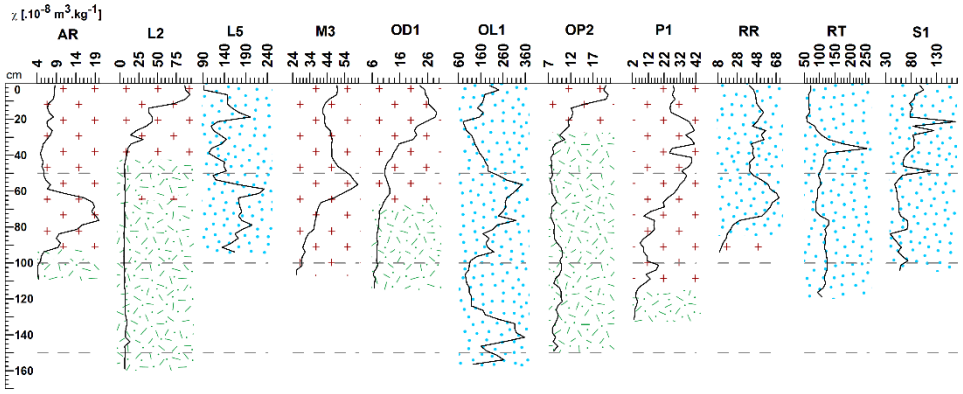

Fig. 4a

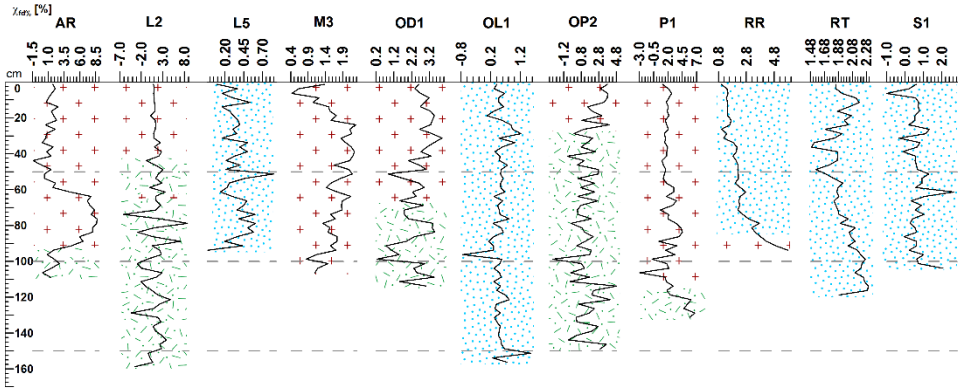

Fig. 4b

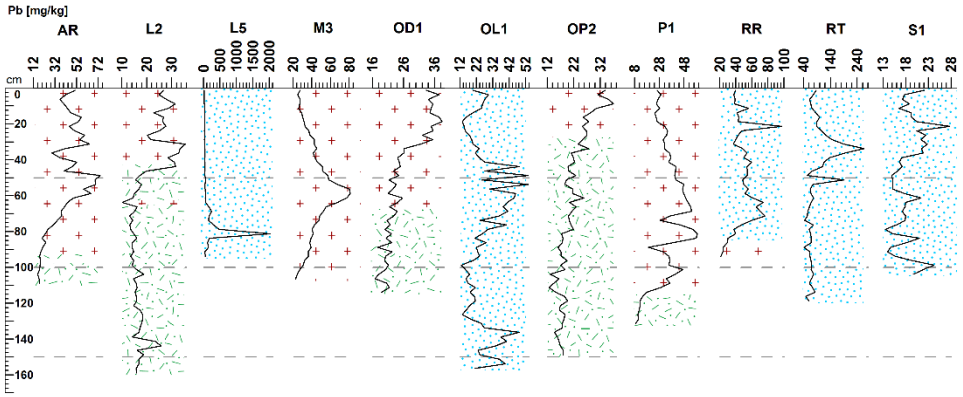

Fig. 4c

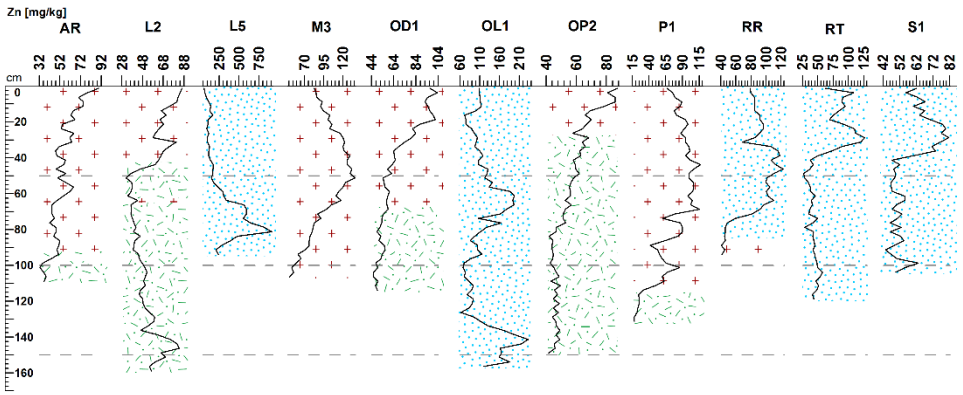

Fig. 4d

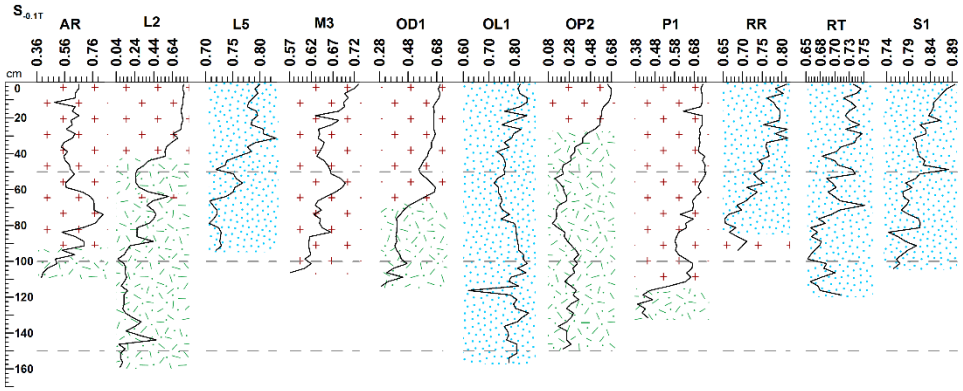

Fig. 4e

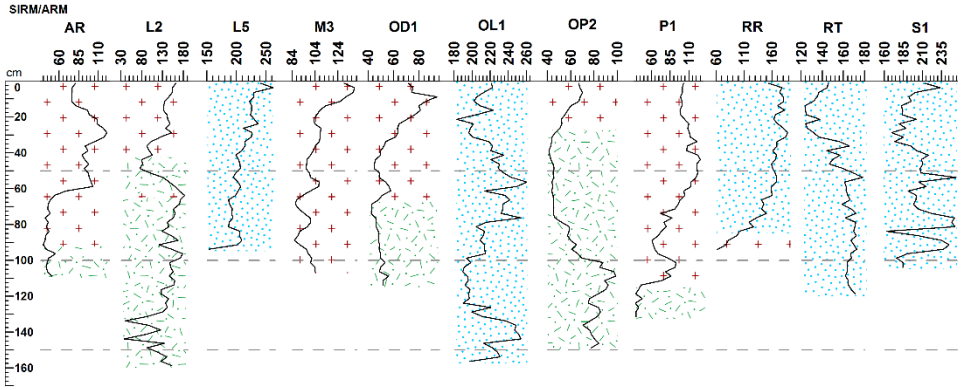

Fig. 4f

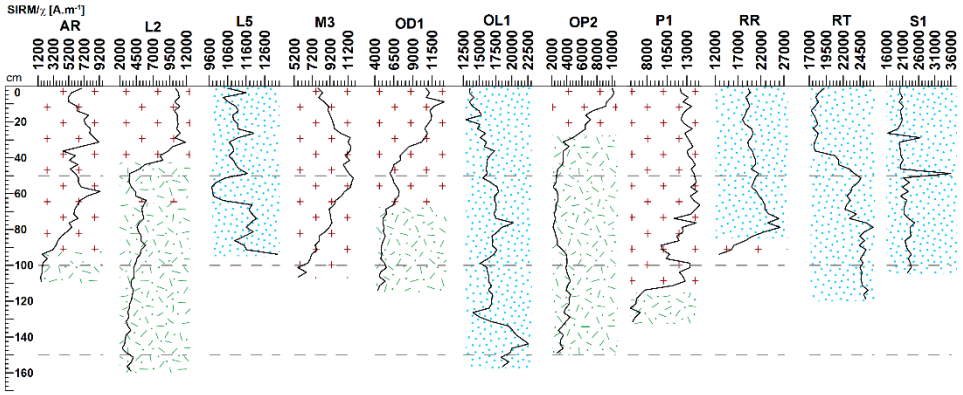

Fig. 4. Depth profiles of the measured parameters: a) magnetic susceptibility (χ), b) frequency-dependent magnetic susceptibility (χfd%)(Note: Sample P1 125 with the extreme value 20.6 % was discarded from the plot to avoid superimposition of the other values), c) concentration of Pb, d) concentration of Zn, e) $S_{-0.1T}$, f) SIRM/ARM ratio and g) SIRM/χ ratio. Note: Colour-shaded background indicates samples' affiliation to the resultant three clusters of k-means clustering: Red crosses = cluster 1, blue dots = cluster 2, and green lines and dots = cluster 3.

k- means, k = 2

cluster 1	cluster 2
L2 32.5-160 OD1 whole OP2 whole M3 whole AR whole P1 2.5-22.5, 27.5-30, 37.5-40, 62.5-132.5 RR 90-95	L2 2.5-30 L5 whole OL1 whole S1 whole RT whole RR 2.5-87.5 P1 25, 32.5-35, 42.5-60

k- means, k = 3

cluster 1	cluster 2	cluster 3
L2 2.5-42.5, 65 OD1 2.5-67.5 OP2 2.5-27.5 M3 whole P1 2.5-115 AR 2.5-92.5, 97.5 RR 87.5-95	OL1 whole S1 whole L5 whole RT whole RR 2.5-85	L2 45-62.5, 67.5-160 OD1 70-115 OP2 30-150 P1 117.5-132.5 AR 95, 100-110

Fig. 5. Resultant separation of samples into clusters by the k-means clustering method with k=2 and k=3.

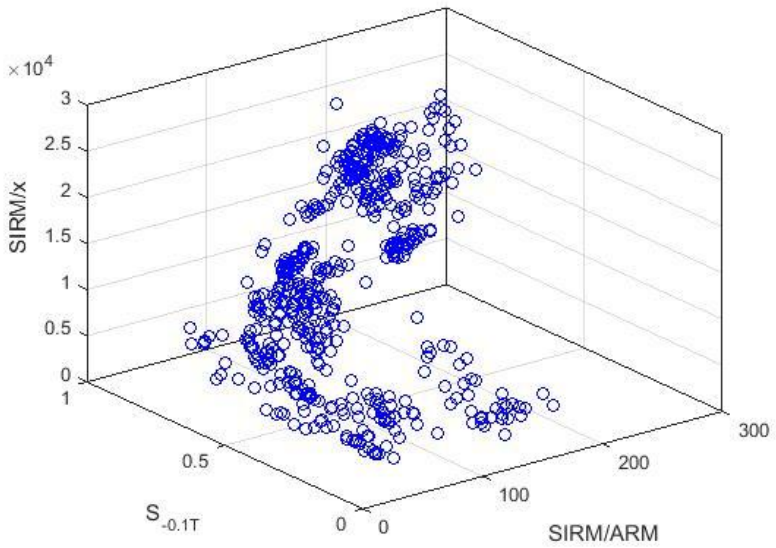

Fig. 6. Pseudo 3D plot visualising the data points' scatter in the clustering space.

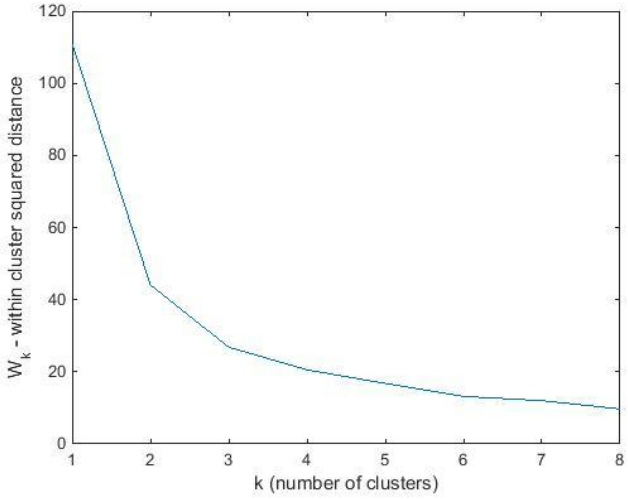

Fig. 7. The so-called Elbow method. Average within cluster squared distance decreases with increasing number of clusters (k). The 'elbow' of the curve, in this case number 3, is the optimal number of clusters.

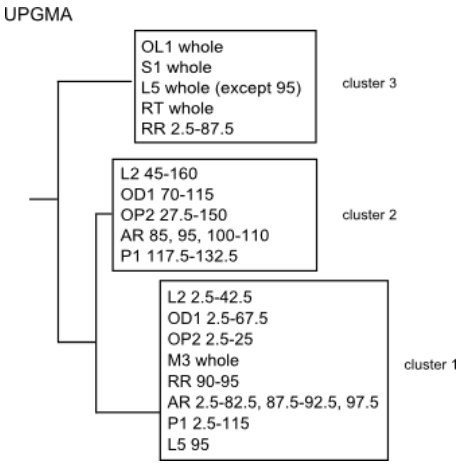

Fig. 8. Simplified dendrogram created by hierarchical clustering method UPGMA. The main branches of the dendrogram are labelled in the same way as the k-means clusters.

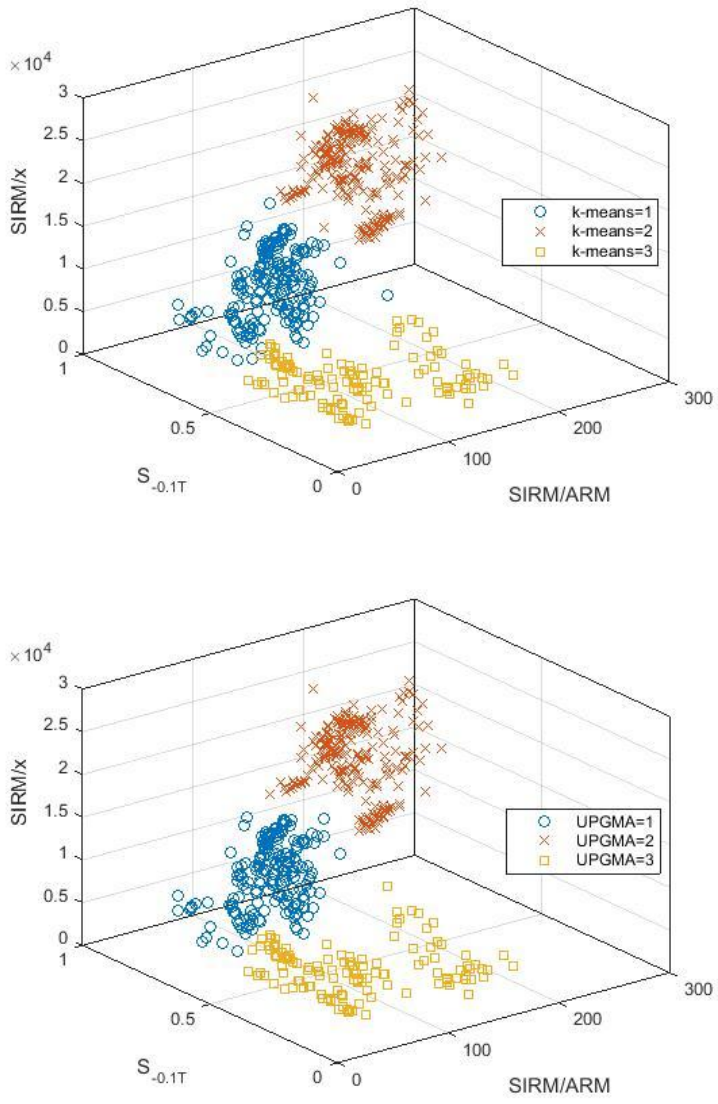

Fig. 9. Pseudo 3D plots depicting clusters distinguished by a) k-means clustering and b) UPGMA method.

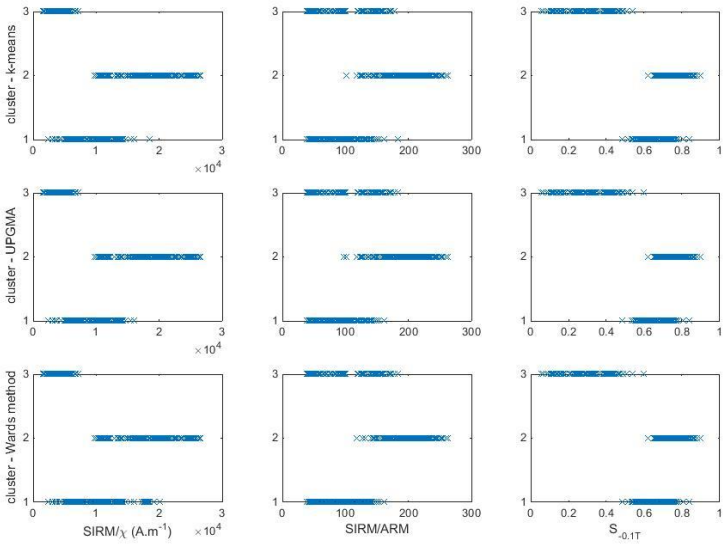

Fig. 10. Graphical expression of the clusters resulting from all three clustering methods using magnetic quotients.

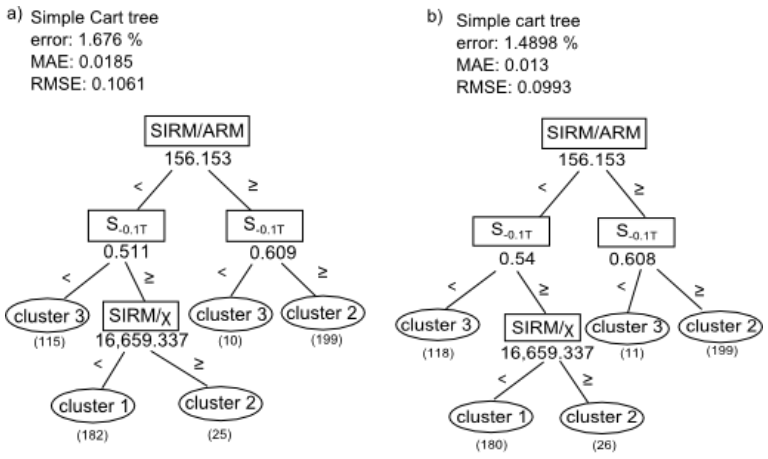

Fig. 11. Decision trees created by the Simple Cart method for a) k-means clusters and b) UPGMA clusters. Note: MAE is the mean absolute error and RMSE is the root-mean-square error. The numbers in brackets indicate the number of samples classified by each tree branch.

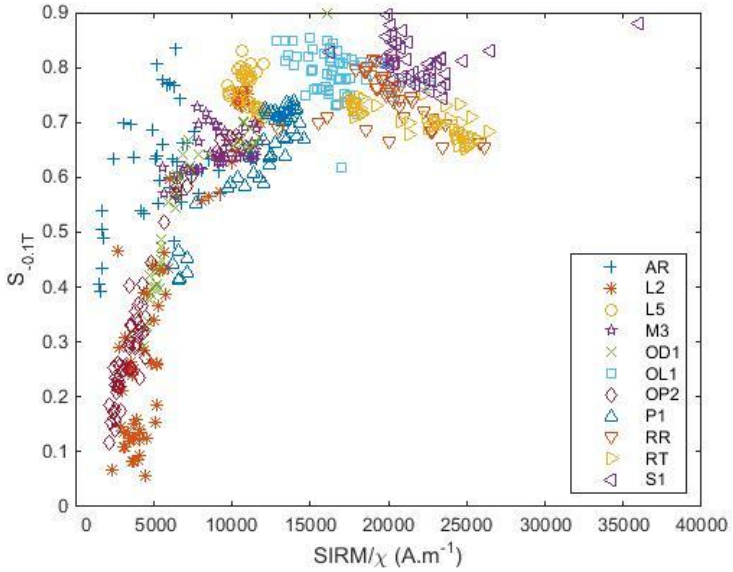

Fig. 12. Relationship between SIRM/χ and $S_{-0.1T}$. All samples analysed are included. The key differentiates samples from each profile.

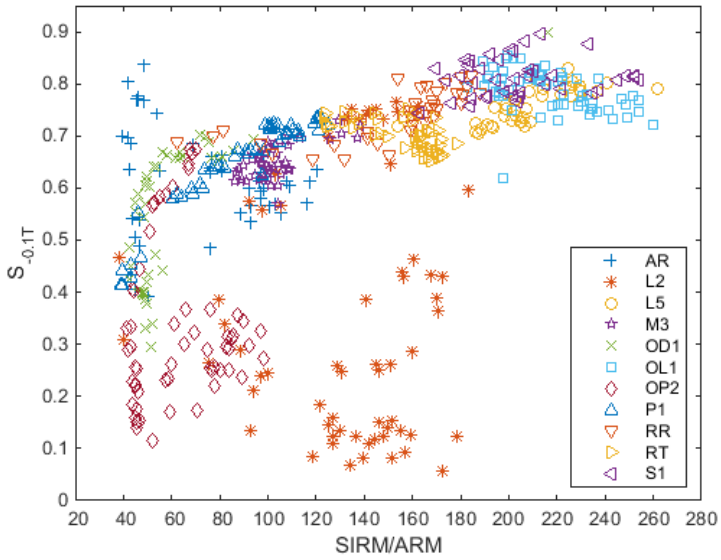

Fig. 13. Relationship between SIRM/ARM and $S_{-0.1T}$. All sampled analysed are included. The key differentiates samples from each profile.

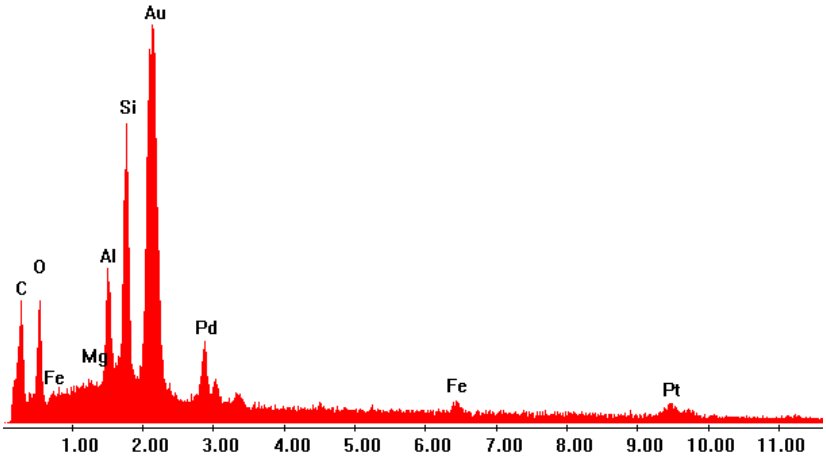

Fig. 14. Energy-dispersive X-ray spectrum of the angular particles in the magnetic extract (visible in Figure 15) obtained using a hand magnet and isopropyl alcohol. Note: Au, Pt and Pd were used for sample coating prior to analysis.

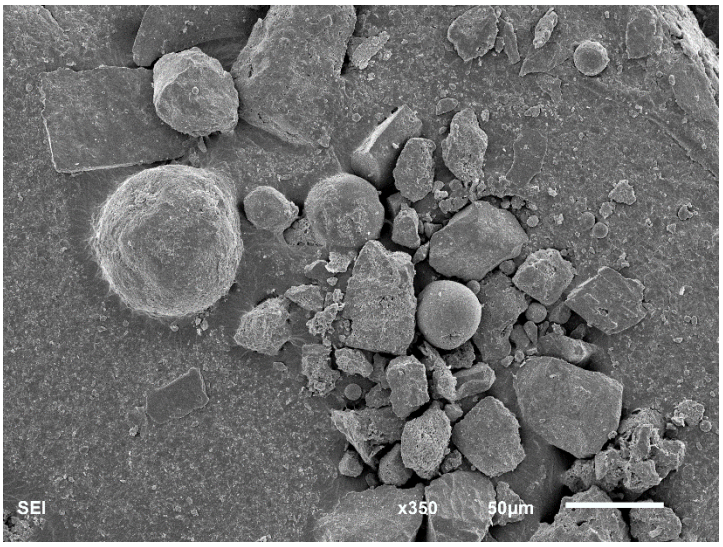

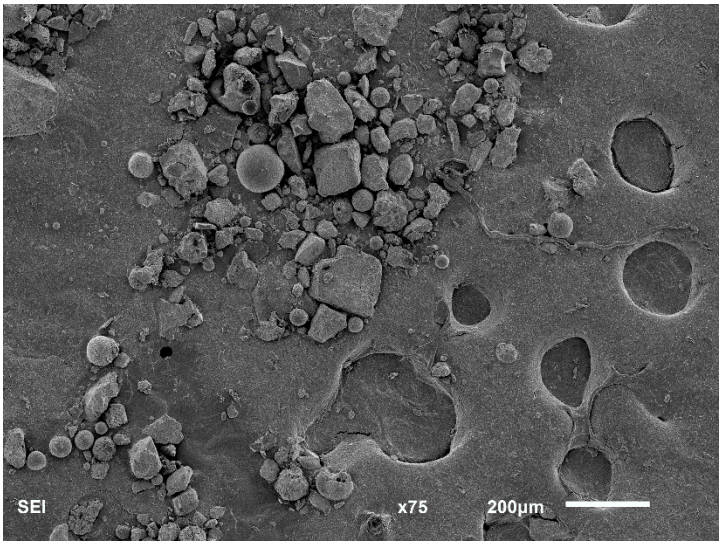

Fig. 15. SEM images showing clusters of spherules originated in combustion processes and angular particles (probably rock fragments) in floodplain sediment. (Magnetic extract for this image was obtained from sample L5 22.5.)

Table 1. Maximal and minimal values of magnetic parameters and other characteristics of the study profiles.

			χ [.10^{-8} m^3.kg^{-1}]		χfd [%]		ARM [.10^{-5} Am^2.kg^{-1}]		SIRM [.10^{-5} Am^2.kg^{-1}]		SIRM/χ [A.m^{-1}]		SIRM/ARM		S-ratio		Pb [mg/kg]		Zn [mg/kg]		organic carbon [%]	
profile	river	coordinates	min	max	min	max	min	max	min	max	min	max	min	max	min	max	min	max	min	max	min	max
L2	Lučina River	N 49.78143 E 018.38603	4.99	93.19	-6.11	8.75	0.10	6.64	13.95	1017.02	2355.83	11873.03	38.38	183.48	0.06	0.77	10.08	35.63	31.84	85.97	3.33	11.67
L5	Lučina River	N 49.82744 E 018.30528	91.43	232.54	-0.03	0.85	4.02	14.05	968.19	2372.15	9721.39	13264.18	153.60	261.95	0.71	0.83	16.41	2035.76	60.48	911.88	2.50	8.33
M3	Morava River	N 49.81065 E 016.93643	25.98	61.71	0.42	2.28	1.41	6.86	146.78	708.14	5561.91	11795.72	85.99	138.17	0.57	0.73	22.57	81.12	51.02	135.67	4.19	9.63
OD1	Odra River	N 49.66202 E 017.98096	6.31	196.11	0.24	3.91	0.57	14.62	28.87	3162.87	4366.85	16128.04	42.47	216.27	0.29	0.90	16.70	38.47	45.54	103.37	1.73	23.58
OL1	Olše River	N 49.87382 E 018.49142	78.94	355.84	-0.75	1.54	6.29	30.69	1186.16	7716.69	12865.31	22583.27	182.71	260.19	0.62	0.85	12.73	53.65	61.80	232.08	1.17	7.83
OP2	Opava River	N 49.90639 E 018.11649	7.31	20.47	-2.43	4.80	0.29	2.97	16.86	202.97	2137.20	10241.01	41.23	98.32	0.12	0.67	12.71	36.94	41.70	87.27	3.99	9.15
P1	Petrůvka River	N 49.90218 E 018.50638	2.70	41.20	-2.95	20.60	0.42	4.91	16.82	566.10	5946.35	14614.66	38.60	125.06	0.39	0.74	8.73	58.78	17.84	117.30	1.66	6.32
S1	Stonávka River	N 49.80236 E 018.53464	38.60	166.45	-0.99	2.65	4.82	20.71	906.66	4280.20	16262.72	35989.33	162.61	254.21	0.74	0.90	13.43	27.73	43.41	81.40	3.70	7.44
AR	Ashop River	N 53.38353 W 001.75339	4.18	19.88	-1.40	8.68	0.14	2.54	6.46	123.20	1530.67	9301.23	39.47	120.58	0.39	0.84	15.94	73.89	32.61	89.35	5.85	31.05
RR	River Ribble	N 54.05358 W 002.29401	9.53	71.07	0.99	5.77	1.98	10.38	123.28	1584.35	12931.99	26119.94	62.31	188.05	0.65	0.81	21.19	96.87	40.53	122.87	2.72	8.50
RT	River Tame	N 53.43909 W 002.14096	57.29	254.56	1.49	2.31	7.92	27.44	1031.57	4546.51	17258.53	26420.18	123.35	178.35	0.65	0.75	40.66	264.96	26.90	126.18	4.88	24.30